# Prospects of $Al_2O_3$ and $MgAl_2O_4$-supported CuO Oxygen Carriers in Chemical-looping Combustion (CLC) and Chemical-looping with Oxygen Uncoupling (CLOU)

*Mehdi Arjmand* [a,*], *Abdul-Majeed Azad* [b,c], *Henrik Leion* [a], *Anders Lyngfelt* [b], *Tobias Mattisson* [b]

[a] Department of Chemical and Biological Engineering, Division of Environmental Inorganic Chemistry, Chalmers University of Technology, SE-412 96 Göteborg, Sweden

[b] Department of Energy and Environment, Chalmers University of Technology, SE-412 96 Göteborg, Sweden

[c] Department of Chemical Engineering, The University of Toledo, Toledo, OH 43606-3390 USA

[*] To whom correspondence should be addressed. Telephone: +46-31-772-28-22;

E-mail: arjmand@chalmers.se

**Abstract**

The chemical-looping combustion (CLC) and chemical-looping with oxygen uncoupling (CLOU) processes are attractive solutions for efficient combustion with direct separation of carbon dioxide. In this work, the feasibility of CuO supported on $Al_2O_3$ and $MgAl_2O_4$ for CLC and CLOU processes are investigated. The oxygen carriers were produced by freeze-granulation and calcined at 950 and 1050°C. The chemical-looping characteristics were evaluated in a laboratory-scale fluidized bed at 900 and 925°C under alternating reducing and oxidizing conditions. Tendencies towards agglomeration, defluidization and loss of active phase were analyzed by changing the experimental process variables, such as reaction time, temperature and reducing and inert environments. Complete conversion of methane was obtained for all oxygen carriers investigated in this work. Three out of four oxygen carriers also featured the rapid release of oxygen in an inert environment (CLOU). In case of $Al_2O_3$ as support, a CLC and a CLOU oxygen carrier were obtained depending on the calcination temperature. In addition, analyses of the CuO-$Al_2O_3$ phase equilibria system under oxidizing and reducing conditions has been carried out. At the investigated temperatures, it is inferred for the case of $Al_2O_3$ as support that part of the active phase (either CuO or $CuAl_2O_4$) is bound as $CuAlO_2$ during incomplete reduction with slow kinetics for re-oxidation. However, when complete reduction is attained, the original active phase composition is rejuvenated upon oxidation. As a result, the use of $CuAl_2O_4$ is suggested for CLC processes from the point of agglomeration and attrition-free functioning of the oxygen carrier. In case of $MgAl_2O_4$ as support, the oxygen carrier exhibited a stable oxygen releasing behavior due to the existence of relatively intact CuO. Together with the absence of agglomeration and major

morphological changes, the use of $MgAl_2O_4$-supported CuO is suggested as a suitable oxygen carrier for CLOU processes.

Keywords: $CO_2$-Capture; Chemical-looping Combustion (CLC); Chemical-looping Combustion with Oxygen Uncoupling (CLOU); Oxygen Carriers; Copper-oxide; Alumina.

## 1. Introduction

As suggested by the intergovernmental panel on climate control (IPCC), a 50-85% reduction in total $CO_2$ emission by 2050 is mandated to limit the anticipated global temperature rise to below 2°C.[1] A number of alternative technologies have been proposed to mitigate the rising levels of carbon dioxide in the atmosphere. Among these, carbon capture and storage (CCS) is considered promising.

The chemical-looping combustion (CLC) process allows intrinsic separation of pure $CO_2$ from a hydrocarbon fuel combustion process. In a CLC system as proposed by Lyngfelt et al.[2], two reactors, viz., fuel and air are interconnected. When fuel and air are introduced into the respective reactor, the following reactions occur

$$(2n+m)Me_xO_y + C_nH_{2m} \rightarrow (2n+m)Me_xO_{y-1} + nCO_2 + mH_2O \quad (1)$$

$$2Me_xO_{y-1} + O_2 \rightarrow 2Me_xO_y \quad (2)$$

Here $Me_xO_y$ and $Me_xO_{y-1}$ are the fully oxidized and reduced forms of the oxygen carrier. The scheme of the process is shown in Figure 1. In case of complete conversion, the exhaust stream from the fuel reactor consists of only $CO_2$ and $H_2O$, from which pure $CO_2$ could be obtained after condensation of water. The reduced form of the oxygen carrier, $Me_xO_{y-1}$, is then transferred to the air reactor where it is re-oxidized by air making it ready for the next cycle. The oxidation

reaction is always exothermic while the reduction reaction can be exothermic or endothermic depending on the nature of the carrier and the fuel.[3] However, the sum of the heat from reaction (1) and (2) is the same as for conventional combustion. Thus the CLC process does not entail additional cost or energy for $CO_2$ separation.

The reactivity of the oxygen carrier during oxidation and reduction cycles and the ability to fully convert the fuel are among the most sought-after criteria. In addition, their thermal stability, mechanical strength, fluidizability and, resistance to attrition and agglomeration are important. In order to achieve this, the active phase is often mixed with an inert support such as $TiO_2$, $SiO_2$, $ZrO_2$, $Al_2O_3$ or $MgAl_2O_4$.[4]

The CLC process could also be achieved through a modification known as chemical-looping with oxygen uncoupling (CLOU)[5]. In comparison to CLC where the reduction of oxygen carrier and oxidation of the gaseous fuel generally occurs in a single step, an additional step is needed in CLOU for the release of gaseous oxygen from the carrier prior to conversion of the fuel according to

$$Me_xO_y \rightarrow Me_xO_{y-2} + O_2 \quad (3)$$

This is followed by the normal combustion of the fuel via

$$C_nH_{2m} + (n + \frac{m}{2})O_2 \rightarrow nCO_2 + mH_2O \quad (4)$$

The reduced oxygen carrier is transferred to the air reactor for re-oxidation. The net heat of reaction for CLOU processes is the same as CLC; only the mechanism by which oxygen is accessed by the fuel differs. However when using solid fuels like coal, the CLOU process avoids the slow gasification of the solid fuel needed to produce syngas as a prerequisite for the reaction with the oxygen carrier.[6] The oxygen carrier in CLOU must be able to release and take up $O_2$ at

temperatures suitable for the process, viz. 800 to 1200°C. This in turn, imposes additional thermodynamic and kinetic requirements on the selected oxygen carrier.

Oxides of transition metals (Mn, Fe, Co, Ni and Cu), their mixtures, and a range of natural ores have been used as oxygen carriers in CLC.[4] Copper-oxide has received a great deal of attention as an efficient oxygen carrier, owing to its high reactivity and oxygen transport capacity and absence of thermodynamic limitation for complete combustion of the fuel. Research has been conducted using copper-oxide as CLC oxygen carrier and methane as fuel in fluidized and fixed bed batch reactors,[7-11] continuous operations[12-15] and thermogravimetric studies,[16-21] with and without the supports mentioned above. Among various supports for CuO oxygen carriers, $Al_2O_3$ has received considerable attention.[10-14, 19, 20, 22]

In addition, CuO decomposes to $Cu_2O$ when the concentration of surrounding oxygen is lower than the equilibrium concentration. As a result, oxygen is released thereby allowing CLOU to take effect. For temperatures of 900 and 925°C, this occurs at oxygen concentrations below 1.5 and 2.7%, respectively.[6] Thus, from a CLOU point of view, the optimum temperature of the air reactor is likely in the range of 900 to 925°C. Some investigations have also attempted to utilize CuO as a CLOU oxygen carrier for the combustion of solid fuels.[6, 23-25]

Despite these attractive features, use of CuO as an oxygen carrier is not without limitations. For example, copper-oxide suffers from the tendency towards agglomeration[10] upon full reduction due to rather low melting temperature of elemental copper (1085°C). Thus the use of low-CuO content (less than 20 wt.%) oxygen carriers was suggested to avoid agglomeration.[10] For the same reason, most of the studies are limited to lower operating temperatures (800-850°C), however with a few exceptions.[12, 13] Although full conversion of methane is achieved even at 800°C, a higher temperature in the fuel reactor is favorable as it increases the equilibrium partial

pressure of $CuO/Cu_2O$, which accompanies the rapid release of oxygen and therefore a higher reactivity.

Moreover in case of $Al_2O_3$ as support, CuO interacts with $Al_2O_3$ either during sample synthesis or in the reactors during operation resulting in partial loss of the active phase.[7, 10, 12-14, 18] Efforts have been made to hinder this interaction by addition of impurities to the $CuO\text{-}Al_2O_3$ mixture, so that free CuO is retained in the bulk.[12]

In cognizance of the potential of copper-based systems as CLC and CLOU materials, a study was undertaken to address two issues concerning the role of $Al_2O_3$ and $MgAl_2O_4$ as a support for CuO in CLC and CLOU applications. Initially, to ascertain a suitable phase boundary in the pseudobinary $CuO\text{-}Al_2O_3$ system for it to behave as a CLC material in light of the fact that there are strong interactions between the two at the typical processing temperatures. Secondly, to investigate the suitability of $MgAl_2O_4$ instead as a support where such active material-support interaction is absent or limited and thus, CuO can function as a suitable CLOU material.

## 2. Experimental

### *2.1 Preparation of Oxygen Carriers*

The oxygen carriers used in this investigation and their physical properties are summarized in Table 1. The particles were manufactured by freeze-granulation. Here, a water-based slurry of CuO and support powders ($\alpha\text{-}Al_2O_3$ and $MgAl_2O_4$) with weight ratio of 40/60 along with small amount of dispersant (Dolapix PC21) is prepared. The mixture is then ball milled for 24 h and binder (Polyvinyl Alcohol) is added prior to granulation. The slurry is pumped through a spray nozzle and into liquid nitrogen to form spherical particles upon instantaneous freezing. The samples were calcined at 950 and 1050°C for 6 h at a ramp rate of 5°C/min and then sieved

through stainless steel screens to yield particles in the range of 125-180 μm. The calcination temperature is given in the abbreviation for each sample as shown in Table 1.

*2.2 Characterization of Oxygen Carriers*

The oxygen carriers were analyzed before and after the experiments using powder X-ray diffraction (Siemens, D5000 Diffractometer) with $CuK_{\alpha}$ radiations. The morphological investigation was carried out with an environmental scanning electron microscope (ESEM) fitted with a field emission gun (FEI, Quanta 200). The BET surface area of the particles was evaluated by $N_2$-absorption (Micromeritics, TriStar 3000). The apparent density of the samples, sized 125-180 μm was measured assuming a void factor of 0.37 as the theoretical voidage of a packed bed with uniform spherical particles. The crushing strength of the particles was also measured as the strength needed to fracture the particles ranging within 180-250 μm for an average of 30 tests per sample using a digital force gauge (Shimpo, FGN-5). The crushing strength was found to be less than 0.5 N for all the samples. In some cases particles with a crushing strength below 1 N are considered too soft.[26] However, this did not cause any problem such as defluidization in the reactor as determined by the pressure drop in the bed. Nonetheless for use in a full scale plant, the crushing strength may need to be increased which could be done by either increasing the sintering time or temperature.

*2.3 Experimental Procedure*

Experiments were carried out in a quartz fluidized-bed reactor, 870 mm long and 22 mm in inner diameter. A porous quartz plate was placed at a height of 370 mm from the bottom and the reactor temperature was measured with chromel-alumel (type K) thermocouples sheathed in

inconel-600 clad located about 5 mm below and 25 mm above the plate. Honeywell pressure transducers with a frequency of 20 Hz were used to measure pressure differences over the bed. The scheme of the experimental setup used in this investigation is shown in Figure 2.

15 g of the oxygen carrier were placed on the porous plate and was then exposed to alternating oxidizing and reducing conditions. The experiment was initiated by heating the reactor to 900°C in 5% $O_2$ in $N_2$ to ensure full oxidation of the carrier prior to the experiments. The use of 5% $O_2$ is to be close to the expected oxygen deficient condition at the air reactor's outlet and also to obviate large temperature increase during the exothermic oxidation when air (21% $O_2$) is employed. A set of three inert gas cycles were initially carried out for all samples in $N_2$ to investigate the release of oxygen during a span of 360 s. For reactivity test, methane was primarily used for 20 s during reduction cycles and repeated for at least three times. The duration of 20 s was selected as it approximately corresponds to the reduction of CuO to $Cu_2O$ only for CLOU processes. Subsequently, additional cycles were carried out in which the reduction time was increased in steps of 10 s intervals up to 70 s. During the prolonged reduction cycles, it is likely that reduction to Cu is gradually approached, i.e. applicable to CLC. The extended reduction time also helped in evaluating the extent to which the active phase was available.

There was no carbon burn-off during the subsequent oxidation cycles (by way of increase in CO and/or $CO_2$ concentrations) to show carbon deposition during shorter reduction cycles. This was due to the fact that more oxygen was available than the stoichiometric demand of the fuel. Depending on the oxygen ratio of the respective sample, some carbon was deposited during the extended reduction cycles as they were depleted of oxygen. However, as the deposition of carbon was not frequent, steam was not incorporated.

Nitrogen was used as an inert purge for 60 s in between oxidation and reduction. The exit gas stream from the reactor was led into a condenser to remove the water. The composition and flow rate of the dry gas was determined on a volumetric base by a Rosemount NGA-2000 analyzer which computed the concentrations of $O_2$, $CO_2$, CO, $CH_4$ and $H_2$. Inlet flow rates of 450, 900 and 600 $mL_N$/min were used during reduction, oxidation and inert cycle, respectively. These flow rates were chosen to achieve values ranging between 12 to 17 $u_{mf}$ during oxidation and, between 4 to 6 $u_{mf}$ during reduction, where $u_{mf}$ is the minimum fluidization velocity.[27]

*2.4 Data Analysis*

The reactivity of a given oxygen carrier is quantified in terms of gas yield or conversion efficiency (γ), and is defined as the fraction of fully oxidized fuel divided by the carbon containing gases in outlet stream, in this work $CO_2$, CO and $CH_4$.

$$\gamma_{red} = \frac{x_{CO_2}}{x_{CO_2} + x_{CH_4} + x_{CO}} \tag{5}$$

Here $x_i$ denotes the composition of the respective gas, obtained from measured concentration in the gas analyzer.

The theoretical oxygen capacity of a given carrier is defined in terms of oxygen ratio ($R_O$), as the maximum mass change of oxygen in the oxygen carrier as follows:

$$R_O = \frac{m_{ox} - m_{red}}{m_{ox}} \tag{6}$$

$m_{ox}$ and $m_{red}$ are the mass of the oxygen carrier in respectively fully oxidized and reduced state.

The conversion of the oxygen carrier, $\omega$, is defined as:

$$\omega = \frac{m}{m_{ox}} \tag{7}$$

$m$ is the actual mass of the oxygen carrier during the experiments.

Equations (8) and (9) are employed for calculating $\omega$ as a function of time during respectively reduction and oxidation period from the measured concentrations of various gaseous species in the gas analyzer:

$$\omega_i = \omega_{i-1} - \int_{t_0}^{t_1} \frac{\dot{n}_{out} M_O}{m_{ox}} \left(4x_{CO_2} + 3x_{CO} + 2x_{O_2} - x_{H_2}\right) dt \tag{8}$$

$$\omega_i = \omega_{i-1} + \int_{t_0}^{t_1} \frac{2M_O}{m_{ox}} \left(\dot{n}_{in} x_{O_2,in} - \dot{n}_{out} x_{O_2,out}\right) dt \tag{9}$$

$\omega_i$ is the instantaneous conversion at time $i$, $\omega_{i-1}$ is the conversion in the preceding instant, $t_0$ and $t_1$ are the initial and final time of measurement. $M_O$ is the molar mass of oxygen and $\dot{n}_{in}$ and $\dot{n}_{out}$ are the dry molar flow rates of the gas at inlet and outlet of the reactor, respectively.

## 3. Results

### *3.1 Concentration Profiles*

Figure 3 shows the oxygen concentration during the inert gas cycle for all samples. During this period, CuO decomposes spontaneously into $Cu_2O$ in the environment of inert nitrogen where the particles release oxygen. The oxygen concentration is relatively consistent with the theoretical equilibrium partial pressure, $p_{O_2}$, corresponding to the decomposition of CuO into $Cu_2O$ (1.5% and 2.7% respectively at 900 and 925$^oC$[6]). This is true for all the carriers tested in this work with the exception of C4A-1050. The insignificant oxygen released from C4A-1050 (0.2%), is further corroborated by the experiments with sand particles, also included in Figure 3 under identical

experimental conditions. As opposed to the C4A-950 particles, the C4A-1050 sample has much less of gaseous oxygen release (CLOU) ability. As seen from Table 1, the only difference between the two materials is the temperature at which they were calcined. Yet, while C4A-950 maintains the anticipated equilibrium oxygen concentration at both operating temperatures, C4A-1050 does only release oxygen to a minor extent. For C4MA-950 and C4MA-1050 samples however, an identical equilibrium concentration of oxygen release is obtained irrespective of the calcination temperature.

Table 2 shows the phase analysis of the fresh and used carriers. The experiments were always ended in the oxidation phase and thus the characterization for the used samples refers to this phase. In case of the C4A-1050 sample, $CuAl_2O_4$ is the predominant phase due to the interaction between copper-oxide and alumina caused by the higher calcination temperature at 1050°C. In the fresh sample, CuO which is capable of releasing oxygen at above 850°C[6], appears as a minor phase together with excess and unreacted alumina. Thus in this case, very little oxygen is released via the CLOU mechanism since $CuAl_2O_4$ is quite incapable of releasing oxygen as shown by the phase evolution of the C4A-1050 material described in section 3.4.

Following the inert gas cycles, successful cycles of oxidation and reduction were carried out for all oxygen carriers. Figure 4 shows the concentration profiles for the C4A-950 sample for the 20 s reduction cycle at 900°C. The decomposition of CuO during the short interval in inert gas prior to fuel injection is due to the spontaneous release of oxygen via the CLOU mechanism. The fuel (methane) reacts exothermically with the released oxygen, producing $CO_2$, with concomitant increase in temperature due to the exothermic nature of the reaction; this is common for copper-based oxygen carriers.[3] The rise in temperature shifts the thermodynamic equilibria and in turn increases the oxygen concentration. However, the actual oxygen concentration during reduction

in the reactor is lower due to dilution created by the water formed. The concentration profiles were similar from cycle to cycle, except for slight variations in peak concentrations due to the transitory non-steady state. At 925°C, more oxygen is released during the inert and reduction cycles.

Rather low oxygen release (~ 0.2%) was seen for the C4A-1050 sample at both 900 and 925°C (Figure 3), compared to the thermodynamically predicted values for the $CuO/Cu_2O$ buffer at these temperatures (about 1.5% and 2.7% respectively at 900 and 925°C[6]). This was attributed to the lesser availability of CuO (Table 2) due to the interaction with the support. Figure 5 shows the concentration profile of C4A-1050 for the 20 s reduction cycle at 925°C. It can be seen that the small oxygen released is completely consumed during the reduction phase, confirming also that not much free CuO existed in C4A-1050. For this reason, $CuAl_2O_4$ which is the major active phase in C4A-1050 does not behave as a CLOU but rather as a CLC material.

The concentration profiles for C4MA-950 and C4MA-1050 samples during 20 s reduction cycles at 900°C were similar to Figure 4. Accordingly at 925°C, more oxygen was released during the inert and reduction cycles. The salient difference between the two profiles was the lower amount of oxygen release for C4MA-950 during reduction.

*3.2 Reactivity of Oxygen Carriers*

Figure 6 shows the reactivity (in terms of gas yield, $\gamma$) of oxygen carriers at 925°C, using methane as the fuel for the third repeated cycle. The point at which $\gamma$ plummets indicates the end of 20 s of reduction. As shown, all samples exhibited high reactivity with complete fuel conversion during this period, irrespective of the temperature at which they were calcined (950 *vs.* 1050°C). The small variation seen in $\omega$ value could be due to normal experimental

fluctuations, possibly in flow measurements. Similar was the development of $\gamma$ *vs.* $\omega$ for reactivity tests at 900°C. The carriers lose approximately 3% of their mass as they are converted during 20 s of reduction ($\omega$ going from 1 to 0.97). During the oxidation cycle that follows, the carrier is expected to retrieve this amount of oxygen, meaning that $\omega$ must revert from 0.97 to 1. Only then, a truly reversible redox behavior of the carrier could be anticipated.

Figure 7 shows the oxygen partial pressure as a function of oxygen carrier conversion, $\omega$, in the oxidation phase following the reduction cycle at 900°C. It can be conceived for C4A-950 that the oxygen partial pressure follows the equilibrium concentration at 1.5% and culminates to 5% while leaving 2% of the oxygen carrier as unconverted as $\omega$ proceeds from 0.97 to 0.98. Note that in Figure 6 approximately 3% of C4A-950 was converted during 20 s of reduction with $\omega$ extending from 1 to 0.97. Similar is the case for C4A-1050, where $\omega$ proceeds from 0.975 to 0.985. The incomplete retrieval of $\omega$ in both cases indicates that part of the active phase (respectively CuO and $CuAl_2O_4$) is lost. However, for the C4MA samples as shown in Figure 7, the carriers retrieved the expected conversion with the value of $\omega$ extending to 1 at the equilibrium oxygen concentration for all oxidation cycles and irrespective of the calcination temperature. This shows that the active CuO phase has remained intact when $MgAl_2O_4$ is used as support.

It is reported that the diffusion of $O_2$ in the depleted oxygen carrier in the oxidation cycle could be hindered by the CuO layer partially surrounding the reduced $Cu_2O$ and Cu grains.[25, 28, 29] Therefore the incomplete oxidation of C4A-950 could initially be connected with this resistance. However, the XRD patterns extracted at the end of experiment for C4A-950 only indicated the oxidized state of the oxygen carrier (i.e. only CuO) together with an increase in the content of $CuAl_2O_4$ and $CuAlO_2$ (Table 2). In addition, the C4A-1050 sample which did not contain a

significant amount of CuO in the fresh state also could not be completely oxidized. Furthermore, the complete regain of $\omega$ in oxidation for the C4MA-950 and C4MA-1050 samples indicates that such resistance in $O_2$ diffusion is not of concern in the oxygen carriers investigated in this work. Thus as will be shown in the phase analysis later (section 3.4), the remaining deficiency in $\omega$ can be attributed to the fact that a part of the active phase is bound in the form of a ternary compound ($CuAlO_2$), that is not readily converted back to the initial composition upon oxidation.

Figure 8 shows the gas yield ($\gamma$) for the C4A-950 and C4MA-950 samples at 925°C during the extended reduction cycle (70 s) with methane. Under the experimental conditions employed, the theoretical conversion of CuO to Cu, $\omega$, at the end of reduction should correspond to 0.92. This was nearly obtained in the case of C4MA-950 and in the case of C4MA-1050 particles (not shown) where it reached a value of 0.93 with full conversion of methane. Reduction times longer than 70 s did not increase the conversion any further for either of the two carriers, confirming that the limit of CuO reduction is reached. On the contrary, in the case of C4A-950, a maximum value of 0.97 was achieved for $\omega$. This leads to the incomplete conversion of methane during the remainder of the cycle, indicating that not as much CuO was available for reduction.

It should also be pointed out that the final prolonged (70 s) reduction cycle was carried out after 16 cycles from the start of the experiment. Thus the high consistency of the mass-based conversion, $\omega$, with the corresponding theoretical value in the case of C4MA samples indicates that the oxidation of $Cu_2O$ to CuO in previous cycles was not subject to any resistance towards $O_2$ diffusion in the depleted CuO layer as suggested previously.[25, 28, 29] In addition, this shows the intact state of the CuO active phase in these materials.

*3.3 Characterization of the Oxygen Carriers*

Characterizations of the oxygen carriers were given in Tables 1 and 2. Among fresh samples, it can be observed for the C4A-1050 particles that the apparent density is lower compared to the C4A-950 sample with the BET value almost unchanged. However, it is worth noting that C4A-1050 had essentially a different chemical composition (predominantly $CuAl_2O_4$) and thus distinct values of apparent density and BET are not unexpected. The BET surface areas of the used samples remained unaltered and did not show any significant variation; the observed small change could be within the experimental error. The post-reaction ESEM images of all samples after the reactivity test are shown in Figure 9 (a-d). Compared to the fresh sample, the used C4A-950 particles exhibited some fragmentation. On the other hand, the surface morphology of the C4A-1050 and C4MA-950 particles did not change appreciably. For the C4MA-1050 sample, most of the particles disintegrated forming considerable amount of debris. The fact that the ESEM micrographs were taken after 17 cycles during which the oxygen carriers were subjected to prolonged reduction, indicates that the C4A-1050 and C4MA-950 oxygen carriers have quite promising mechanical resistance.

It is clear that both systems show high reactivity (Figure 6). The $MgAl_2O_4$-supported carrier has the advantage of no or limited interaction between CuO and the $MgAl_2O_4$ support. This is true for both oxidizing and reducing experiments in the temperature regime of investigation (Table 2). Thus, from the foregoing set of observations it can be inferred that C4MA-950 is a suitable oxygen carrier for CLOU processes. This is corroborated by stable and consistent release of oxygen (Figure 3), invariant amount of CuO (Figure 8) and, absence of agglomeration and major morphological changes that were seen in the case of C4MA-950 (Figure 9).

The $Al_2O_3$-supported system is somewhat complicated due to the phase formation probability in the regime of processing as well as application temperatures. The loss of CuO active phase due

to formation of $CuAlO_2$ in C4A-950 (Figure 7 and 8) raises questions about the long-term stability of this oxygen carrier as a CLOU material. On the other hand, C4A-1050 is recognized as a CLC material (Figure 5), though alike C4A-950, the active phase (in this case $CuAl_2O_4$) is not fully obtained upon oxidation (Figure 7). The phase-field shift in the CuO-$Al_2O_3$ system sheds light on the observed difficulty in the reversible behavior of $Al_2O_3$-supported CuO oxygen carriers, as discussed below.

*3.4 Phase Equilibria Analysis for $Al_2O_3$-supported CuO Oxygen Carriers*

The relationship among various components in the pseudobinary CuO ($Cu_2O$)-$Al_2O_3$ system is of great relevance to CLC and/or CLOU processes concerning the $Al_2O_3$-supported CuO oxygen carriers. The CuO-$Al_2O_3$ phase diagram was reported at atmospheric pressure ( $p_{O_2}$ = 0.21 atm.) by Gadalla and White[30] and further developed by Jacob and Alcock.[31] Based on the method of synthesis (bulk oxide reaction versus thin film formation), considerable disagreements exist as to the accuracy of phase formation and transformation.[32-36] However, the operative boundaries for the CLC and/or CLOU processes could be defined quite accurately without any ambiguity. For example, irrespective of the modification of the alumina used (such as $\alpha$, $\gamma$, $\eta$ or $\theta$, etc.) during material synthesis, the $CuAl_2O_4$ spinel is invariably formed at high temperatures (above 1000$^o$C)[37-39] as per the solid-state reaction:

$$CuO + Al_2O_3 \rightarrow CuAl_2O_4 \qquad (10)$$

However, the interaction between copper-oxide and $\gamma$-$Al_2O_3$ is much faster and occurs at even much lower temperatures (above 600$^o$C), compared to that with $\alpha$-$Al_2O_3$ owing to large surface area and better reaction kinetics.[38-40] Thus, in the case of C4A-950, the active phase and support

remained individual components and copper (II) aluminate, $CuAl_2O_4$, was found only as a minor phase in the fresh material, as shown in Table 2.

At around 1026°C, CuO decomposes into $Cu_2O$ in air, which in turn reacts with free alumina phase to form copper (I) aluminate, delafossite ($CuAlO_2$):

$$Cu_2O + Al_2O_3 \rightarrow 2CuAlO_2 \quad (11)$$

Between 1050 and 1170°C in an $Al_2O_3$-rich mixture, $CuAlO_2$ is metastable in air and transforms into $CuAl_2O_4$, via the following reversible reaction[38, 40, 41]

$$4CuAlO_2 + 2Al_2O_3 + O_2 \leftrightarrow 4CuAl_2O_4 \quad (12)$$

Thus, in the case of C4A-1050, $CuAl_2O_4$ was formed as the major phase upon calcination at 1050°C (Table 2). Visual examination of the C4A-950 and C4A-1050 samples also helps in identifying the phases: C4A-950 which consisted mainly of CuO and $Al_2O_3$ had the appearance of grey to black. On the other hand, C4A-1050 was orange; the color of $CuAl_2O_4$.[42]

Annealing of thin copper films deposited on alumina substrates, in nitrogen[33] shows that $CuAl_2O_4$ spinel could be reduced to $CuAlO_2$ as per reverse of reaction (12). However, as shown in Figure 3, $CuAl_2O_4$ in C4A-1050 sample does not release oxygen at a significant level in an inert atmosphere at 900-925°C. Nonetheless, it can still be reduced by methane as demonstrated in Figure 5 and reported elsewhere using thermogravimetric studies[18] and temperature programmed reduction (TPR).[42]

Recently, Kumekawa et al.[32] reported the T- $p_{O_2}$ boundaries for the CuO-$CuAl_2O_4$-$CuAlO_2$ phase fields. It was shown that $CuAlO_2$ is thermodynamically stable in air above 900°C, but that it undergoes the following kinetically hindered decomposition below 900°C.

$$2CuAlO_2 + \frac{1}{2}O_2 \rightarrow CuO + CuAl_2O_4 \quad (13)$$

In the light of the reaction pathways between CuO and $Al_2O_3$ and using the Gibbs energy data reported by Gadalla and White[30] and Jacob and Alcock[31] the phase relationships as a function of oxygen partial pressure in the temperature range of relevance could be established. This is shown in Figure 10 after Ingram et al.[43] at atmospheric pressure.

According to Figure 10 at $p_{O_2}$ = 0.05 atm., the amount of $CuAl_2O_4$ (a minor phase in fresh C4A-950) increases by way of reaction (10) with increasing temperature. In case of C4A-950, CuO is amenable to decomposition into $Cu_2O$ under the prevailing conditions of low $p_{O_2}$ at 900 or 925°C in the fuel reactor and during the inert cycles. This is then likely to promote the reaction with alumina, leading to the formation of $CuAlO_2$ via reaction (11). In case of C4A-1050, $CuAl_2O_4$ is reduced by methane resulting also in the formation of $CuAlO_2$. In either case, subsequent oxidation does not readily transform $CuAlO_2$ into $CuAl_2O_4$ or CuO via reaction (12) or (13). This is because the temperature is lower than required for reaction (12) to proceed and because reaction (13) is kinetically slow as mentioned above. This explains the presence of $CuAlO_2$ after oxidation for both samples, as evidenced from the XRD analysis in Table 2 and corroborated by Figure 7. It also shows that subsequent to reduction, the carriers were not completely oxidized to the original composition. Thus, the loss of active phase (CuO or $CuAl_2O_4$) could be related to the formation and increase of the $CuAlO_2$ phase.

To further investigate the CuO-$Al_2O_3$ phase equilibria, it was argued that if the reduction was to proceed so as to yield elemental Cu, one could conceivably reclaim the initial composition again upon oxidation without going through the kinetically hindered transformation involving $CuAlO_2$. This probability was initially tested by using an independent reduction scheme with $H_2$ (instead of $CH_4$) to avoid the formation of coke. The systematic phase evolution in the reduction and oxidation cycles for C4A-950 is shown in Figure 11. The $H_2$-reduced sample (Cu and $Al_2O_3$)

could be successfully oxidized to a mixture of CuO and $Al_2O_3$, identical to that of the fresh sample. However, there was evidence of agglomeration, as seen from the ESEM images of the oxidized sample shown in Figure 12 (a).

For C4A-1050, a similar scheme was used. In this case, a long (approximately 4 h) $N_2$-inert cycle was used prior to $H_2$-reduction. The low release of oxygen from the small amount of CuO (Table 2) as seen in Figure 3 was noticed again, which eventually declined to zero during the long inert period. The reactor was cooled in $N_2$ and the XRD pattern collected at this extreme indicated the presence of $Cu_2O$, $Al_2O_3$, and $CuAl_2O_4$ only. The phase analysis of the following $H_2$-reduced specimen revealed the presence of Cu and $Al_2O_3$. Upon oxidation in 5% $O_2$ stream, a diffraction pattern identical to that of the fresh C4A-1050 sample was obtained (Figure 13). Thus, the carrier was effectively oxidized without going through the kinetically hindered phase transformation involving $CuAlO_2$ as per reaction (13). Note that at $p_{O_2}$ = 0.05 atm., the formation of $CuAl_2O_4$ from constituent oxides is thermodynamically feasible even at 900°C (Figure 10).

An attempt was also made to re-oxidize the fully-reduced C4A-1050 (Cu and $Al_2O_3$ mixture) in air, assuming that it would oxidize elemental copper fully to CuO (Figure 10). However, the $CuAl_2O_4$ and $Al_2O_3$ phase mixture was obtained again. Ertl et. al.[44] observed the formation of $CuAl_2O_4$ upon oxidation of a Cu and $Al_2O_3$ mixture at 400°C in 16% $O_2$. It was suggested that Cu is initially oxidized to CuO, but the highly disordered and reactive state of CuO and $Al_2O_3$ particles caused by the redox cycles transforms the mixture into the original spinel even at such low temperatures. For this reason and since reaction (12) is completed at above 1050°C, at which C4A-1050 was originally calcined, the possible mechanism for the formation of $CuAl_2O_4$ at 900°C in both cases ( $p_{O_2}$ = 0.05 and 0.21 atm.) is via reaction (10).

Surprisingly, there was no agglomeration of the bed in either of the oxidation cases for the C4A-1050 sample. The ESEM image of the oxidized C4A-1050 particles is shown in Figure 12 (b), which shows quite distinct morphological features. The most striking aspect is the extreme smoothness of the particle surfaces, uniformity of the granules and lack of fine formation in comparison to that observed for C4A-950.

The decomposition of $CuAlO_2$ though kinetically hindered, can be accelerated if oxidation is carried out in air, i.e. 21% $O_2$. To illustrate this, oxidation of 5 g of the used C4A-1050 sample (containing considerable amount of $CuAlO_2$; Table 2) was carried out for about 1½ h at 900$^o$C in air. This yielded a mixture of $CuAl_2O_4$, $Al_2O_3$ and CuO with the amount of CuO higher (7.5%) compared to the fresh C4A-1050 sample (1.5%) as determined by the XRD; this is in agreement with reaction (13). The color of this sample was chocolate brown due to the increase in CuO content compared to that of fresh C4A-1050 or the one oxidized from fully reduced C4A-1050 (orange), both of which were predominantly composed of $CuAl_2O_4$. Although in a CLC unit air is used for oxidation, it should be emphasized that the oxygen concentration at the air reactor's outlet is lower, thus part of the $CuAlO_2$ phase will likely remain from completely decomposing to CuO and $CuAl_2O_4$.

*3.5 Agglomeration and Attrition Resistance Attributes of $CuAl_2O_4$*

It was observed that the C4A-1050 sample did not agglomerate when fully reduced and re-oxidized. Thus to further evaluate the attrition resistance of $CuAl_2O_4$, a multi-cycle test (additional 5 cycles) of C4A-1050, was carried out using methane at 900$^o$C to simulate a more realistic condition in CLC. Neither agglomeration nor defluidization was encountered. It was possible to completely reduce the oxygen carrier in methane and fully oxidize it in 5% $O_2$ in a

similar manner shown in Figure 13. This negates the concern over the possibility of reducing $CuAl_2O_4$ to Cu and $Al_2O_3$ using methane as fuel. The ESEM analyses on the C4A-1050 subjected to the multi-cycle test are shown in Figure 14; any sign of agglomeration or the presence of fines are absent.

In light of this, the use of $CuAl_2O_4$ can be suggested for CLC processes due to agglomeration and attrition resistance of this oxygen carrier. The oxygen ratio for various phases in the Cu-Al-O system is shown in Table 3. It was previously found that employing a low amount of CuO (less than 20 wt.%) by impregnation in $Al_2O_3$ helps to avoid agglomeration.[10] In such case, the oxygen ratio would be lower than pure $CuAl_2O_4$, given its higher copper content.

## 4. Conclusion

The conclusions drawn from this work are as follows. For $Al_2O_3$-supported CuO oxygen carriers calcined at 950$^o$C and 1050$^o$C, it is inferred from analysis of the phase equilibria at above 900$^o$C that:

(1) part of the active phase (respectively CuO and $CuAl_2O_4$) is bound as $CuAlO_2$ during incomplete reduction with slow kinetics for re-oxidation. This results in partial loss of the active phase after several redox cycles.

(2) if complete reduction is attained, the original active phase composition can be rejuvenated. In this case, the use of $CuAl_2O_4$ as an oxygen carrier can be suggested for CLC processes due to resistance against agglomeration and attrition. Moreover, $CuAl_2O_4$ spinel has a higher oxygen transport capacity than low-CuO loading on $Al_2O_3$ support oxygen carriers.

For $MgAl_2O_4$-supported CuO oxygen carriers, it is concluded that the active CuO phase is retained by avoiding the interaction between CuO and $Al_2O_3$ thus offering a stable oxygen release

capacity due to existence of relatively intact CuO. Together with the absence of major morphological changes, the $MgAl_2O_4$-supported CuO appears as a suitable oxygen carrier for CLOU processes, although long-term validation of their use with solid fuels and in continuous operation is needed.

**Acknowledgments**

The authors wish to thank Vattenfall and Chalmers University of Technology via the Energy Area of Advance for the financial support of this work. One of the authors (AMA) wishes to thank the United States Council for International Exchange of Scholars for the 2010/11 Fulbright Distinguished Chair Award in Alternative Energy Technology.

**References**

(1) IPCC *Fourth Assesment Report: Climate Change*; Intergovernmental Panel on Climate Change: 2007.
(2) Lyngfelt, A.; Leckner, B.; Mattisson, T., A fluidized-bed combustion process with inherent $CO_2$ separation; application of chemical-looping combustion. *Chemical Engineering Science* **2001,** 56, (10), 3101-3113.
(3) Jerndal, E.; Mattisson, T.; Lyngfelt, A., Thermal Analysis of Chemical-Looping Combustion. *Chemical Engineering Research and Design* **2006,** 84, (9), 795-806.
(4) Hossain, M. M.; de Lasa, H. I., Chemical-looping combustion (CLC) for inherent $CO_2$ separations-a review. *Chemical Engineering Science* **2008,** 63, (18), 4433-4451.
(5) Lyngfelt, A., Mattisson, T Trestegsförbränning för avskiljning av koldioxid. 2005.
(6) Mattisson, T.; Lyngfelt, A.; Leion, H., Chemical-looping with oxygen uncoupling for combustion of solid fuels. *International Journal of Greenhouse Gas Control* **2009,** 3, (1), 11-19.
(7) Cho, P.; Mattisson, T.; Lyngfelt, A., Comparison of iron-, nickel-, copper- and manganese-based oxygen carriers for chemical-looping combustion. *Fuel* **2004,** 83, (9), 1215-1225.
(8) Corbella, B. M.; De Diego, L.; García, F.; Adánez, J.; Palacios, J. M., The Performance in a Fixed Bed Reactor of Copper-Based Oxides on Titania as Oxygen Carriers for Chemical Looping Combustion of Methane. *Energy & Fuels* **2005,** 19, (2), 433-441.
(9) Corbella, B. M.; de Diego, L.; García-Labiano, F.; Adánez, J.; Palacios, J. M., Characterization and Performance in a Multicycle Test in a Fixed-Bed Reactor of Silica-Supported Copper Oxide as Oxygen Carrier for Chemical-Looping Combustion of Methane. *Energy & Fuels* **2005,** 20, (1), 148-154.

(10) de Diego, L. F.; Gayán, P.; García-Labiano, F.; Celaya, J.; Abad, A.; Adánez, J., Impregnated $CuO/Al_2O_3$ Oxygen Carriers for Chemical-Looping Combustion: Avoiding Fluidized Bed Agglomeration. *Energy & Fuels* **2005,** 19, (5), 1850-1856.
(11) Chuang, S. Y.; Dennis, J. S.; Hayhurst, A. N.; Scott, S. A., Development and performance of Cu-based oxygen carriers for chemical-looping combustion. *Combustion and Flame* **2008,** 154, (1-2), 109-121.
(12) Gayán, P.; Forero, C. R.; Abad, A.; de Diego, L. F.; García-Labiano, F.; Adánez, J., Effect of Support on the Behavior of Cu-Based Oxygen Carriers during Long-Term CLC Operation at Temperatures above 1073 K. *Energy & Fuels* **2011,** 25, (3), 1316–1326.
(13) Forero, C. R.; Gayán, P.; García-Labiano, F.; de Diego, L. F.; Abad, A.; Adánez, J., High temperature behaviour of a $CuO/\gamma Al_2O_3$ oxygen carrier for chemical-looping combustion. *International Journal of Greenhouse Gas Control* **2011,** 5, (4), 659-667.
(14) de Diego, L. F.; GarcI´a-Labiano, F.; Gayán, P.; Celaya, J.; Palacios, J. M.; Adánez, J., Operation of a 10 kWth chemical-looping combustor during 200 h with a $CuO-Al_2O_3$ oxygen carrier. *Fuel* **2007,** 86, (7-8), 1036-1045.
(15) Adánez, J.; Gayán, P.; Celaya, J.; de Diego, L. F.; García-Labiano, F.; Abad, A., Chemical Looping Combustion in a 10 kWth Prototype Using a $CuO/Al_2O_3$ Oxygen Carrier: Effect of Operating Conditions on Methane Combustion. *Industrial & Engineering Chemistry Research* **2006,** 45, (17), 6075-6080.
(16) Zafar, Q.; Mattisson, T.; Gevert, B., Redox Investigation of Some Oxides of Transition-State Metals Ni, Cu, Fe, and Mn Supported on $SiO_2$ and $MgAl_2O_4$. *Energy & Fuels* **2005,** 20, (1), 34-44.
(17) Adánez, J.; de Diego, L. F.; García-Labiano, F.; Gayán, P.; Abad, A.; Palacios, J. M., Selection of Oxygen Carriers for Chemical-Looping Combustion. *Energy & Fuels* **2004,** 18, (2), 371-377.
(18) de Diego, L. F.; GarcIa-Labiano, F.; Adánez, J.; Gayán, P.; Abad, A.; Corbella, B. M.; MarIa Palacios, J., Development of Cu-based oxygen carriers for chemical-looping combustion. *Fuel* **2004,** 83, (13), 1749-1757.
(19) Noorman, S.; Gallucci, F.; van Sint Annaland, M.; Kuipers, H. J. A. M., Experimental Investigation of a $CuO/Al_2O_3$ Oxygen Carrier for Chemical-Looping Combustion. *Industrial & Engineering Chemistry Research* **2010,** 49, (20), 9720-9728.
(20) Mattisson, T.; Järdnäs, A.; Lyngfelt, A., Reactivity of Some Metal Oxides Supported on Alumina with Alternating Methane and OxygenApplication for Chemical-Looping Combustion. *Energy & Fuels* **2003,** 17, (3), 643-651.
(21) Adánez, J.; García-Labiano, F.; de Diego, L. F.; Gayán, P.; Celaya, J.; Abad, A., Nickel–Copper Oxygen Carriers To Reach Zero CO and $H_2$ Emissions in Chemical-Looping Combustion. *Industrial & Engineering Chemistry Research* **2006,** 45, (8), 2617-2625.
(22) Son, S. R.; Go, K. S.; Kim, S. D., Thermogravimetric Analysis of Copper Oxide for Chemical-Looping Hydrogen Generation. *Industrial & Engineering Chemistry Research* **2008,** 48, (1), 380-387.
(23) Mattisson, T.; Leion, H.; Lyngfelt, A., Chemical-looping with oxygen uncoupling using $CuO/ZrO_2$ with petroleum coke. *Fuel* **2009,** 88, (4), 683-690.
(24) Cao, Y.; Pan, W.-P., Investigation of Chemical Looping Combustion by Solid Fuels. 1. Process Analysis. *Energy & Fuels* **2006,** 20, (5), 1836-1844.

(25) Eyring, E. M.; Konya, G.; Lighty, J. S.; Sahir, A. H.; Sarofim, A. F.; Whitty, K., Chemical Looping with Copper Oxide as Carrier and Coal as Fuel. *Oil & Gas Science and Technology – Rev. IFP Energies nouvelles* **2011,** 66, (2), 209-221.
(26) Johansson, M.; Mattisson, T.; Lyngfelt, A., Investigation of $Fe_2O_3$ with $MgAl_2O_4$ for Chemical-Looping Combustion. *Industrial & Engineering Chemistry Research* **2004,** 43, (22), 6978-6987.
(27) Kunni, D.; Levenspiel, O., *Fluidization Engineering*. Butterworth-Heinemann: 1991.
(28) Chuang, S. Y.; Dennis, J. S.; Hayhurst, A. N.; Scott, S. A., Kinetics of the Oxidation of a Co-precipitated Mixture of Cu and $Al_2O_3$ by O2 for Chemical-Looping Combustion. *Energy & Fuels* **2010,** 24, (7), 3917-3927.
(29) Chadda, D.; Ford, J. D.; Fahim, M. A., Chemical Energy Storage by the Reaction Cycle CuO/$Cu_2O$ *International Journal of Energy Research* **1989,** 13, (63), 73.
(30) Gadalla, A. M. M.; White, J., Equilibrium Relationships in the System CuO-$Cu_2O$-$Al_2O_3$. *J. Brit. Ceram. Soc.* **1964,** 63, (1), 39-62.
(31) Jacob, K. T.; Alcock, C. B., Thermodynamics of $CuAlO_2$ and $CuAl_2O_4$ and Phase Equilibria in the System $Cu_2O$-CuO-Al2$O_3$. *Journal of the American Ceramic Society* **1975,** 58, (5-6), 192-195.
(32) Kumekawa, Y.; Hirai, M.; Kobayashi, Y.; Endoh, S.; Oikawa, E.; Hashimoto, T., Evaluation of thermodynamic and kinetic stability of $CuAlO_2$ and $CuGaO_2$. *Journal of Thermal Analysis and Calorimetry* **2010,** 99, (1), 57-63.
(33) Tsuboi, N.; Itoh, Y.; Ogata, J.; Kobayashi, S.; Shimizu, H.; Kato, K.; Kaneko, F., Composition and Structure Control of Cu–Al–O Films Prepared by Reactive Sputtering and Annealing. *Japanese Journal of Applied Physics* **2007,** 46, (1), 351–355.
(34) Okada, K.; Hattori, A.; Taniguchi, T.; Nukui, A.; Das, R. N., Effect of Divalent Cation Additives on the γ-$Al_2O_3$-to-α-$Al_2O_3$ Phase Transition. *Journal of the American Ceramic Society* **2000,** 83, (4), 928-932.
(35) Cai, J.; Gong, H., The influence of Cu/Al ratio on properties of chemical-vapor-deposition-grown p-type Cu–Al–O transparent semiconducting films. *Journal of Applied Physics* **2005,** 98, (3), 033707-033707-5.
(36) Misra, S. K.; Chaklader, A. C. D., The System Copper Oxide—Alumina. *Journal of the American Ceramic Society* **1963,** 46, (10), 509-509.
(37) Tsuchida, T.; Furuichi, R.; Sukegawa, T.; Furudate, M.; Ishii, T., Thermoanalytical study on the reaction of the CuO-$Al_2O_3$ (η, γ, and α) systems. *Thermochimica Acta* **1984,** 78, (1-3), 71-80.
(38) Bolt, P. H.; Habraken, F. H. P. M.; Geus, J. W., Formation of Nickel, Cobalt, Copper, and Iron Aluminates from α- and γ-Alumina-Supported Oxides: A Comparative Study. *Journal of Solid State Chemistry* **1998,** 135, (1), 59-69.
(39) Tang, Y.; Chui, S. S.-Y.; Shih, K.; Zhang, L., Copper Stabilization via Spinel Formation during the Sintering of Simulated Copper-Laden Sludge with Aluminum-Rich Ceramic Precursors. *Environmental Science & Technology* **2011,** 45, (8), 3598–3604.
(40) Susnitzky, D. W.; Carter, C. B., The formation of copper aluminate by solid-state reaction. *Journal of Materials Research* **1991,** 6, (09), 1958-1963
(41) Hu, C.-Y.; Shih, K.; Leckie, J. O., Formation of copper aluminate spinel and cuprous aluminate delafossite to thermally stabilize simulated copper-laden sludge. *Journal of Hazardous Materials* **2010,** 181, (1-3), 399-404.

(42) Woelk, H.-J.; Hoffmann, B.; Mestl, G.; Schloegl, R., Experimental Archaeology: Investigation on the Copper–Aluminum–Silicon–Oxygen System. *Journal of the American Ceramic Society* **2002,** 85, (7), 1876-1878.
(43) Ingram, B. J.; Mason, T. O.; Asahi, R.; Park, K. T.; Freeman, A. J., Electronic structure and small polaron hole transport of copper aluminate. *Physical Review B* **2001,** 64, (15), 155114.
(44) Ertl, G.; Hierl, R.; Knözinger, H.; Thiele, N.; Urbach, H. P., XPS study of copper aluminate catalysts. *Applications of Surface Science* **1980,** 5, (1), 49-64.

**Table 1.** Oxygen carrier's properties

| Oxygen Carrier | C4A-950 | C4A-1050 | C4MA-950 | C4MA-1050 |
|---|---|---|---|---|
| Theoretical CuO content [wt.%] | 40 | | | |
| Support phase | $\alpha$-$Al_2O_3$ (A16SG, Alcoa) | | $MgAl_2O_4$ (S30CR, Baikowski) | |
| Size interval of particles [µm] | 125-180 | | | |
| Apparent density [g/cm$^3$] | 2.4 | 1.8 | 2.1 | 2.6 |
| BET specific surface area [m$^2$/g] | 4.1 | 4.2 | 11.7 | 6.5 |
| Crushing strength [N] | < 0.5 | | | |

**Table 2.** Phase analysis of the oxygen carriers

| | Identified phases | |
|---|---|---|
| | Fresh samples | Used samples |
| C4A-950 | CuO, $\alpha$-$Al_2O_3$, $CuAl_2O_4$* | CuO, $\alpha$-$Al_2O_3$, $CuAl_2O_4$, $CuAlO_2$ |
| C4MA-950 | CuO, $MgAl_2O_4$ | CuO, $MgAl_2O_4$ |
| C4A-1050 | $CuAl_2O_4$, $\alpha$-$Al_2O_3$, CuO* | $CuAl_2O_4$, $CuAlO_2$, $\alpha$-$Al_2O_3$ |
| C4MA-1050 | CuO, $MgAl_2O_4$ | CuO, $MgAl_2O_4$ |

* Minor phase

**Table 3.** Theoretical oxygen ratio of copper derivatives

| | $R_O$ (%) |
|---|---|
| CuO/Cu | 20.1 |
| $Cu_2O$/Cu | 11.2 |
| CuO/$Cu_2O$ | 10 |
| $CuAl_2O_4$/Cu (+$Al_2O_3$) | 8.8 |

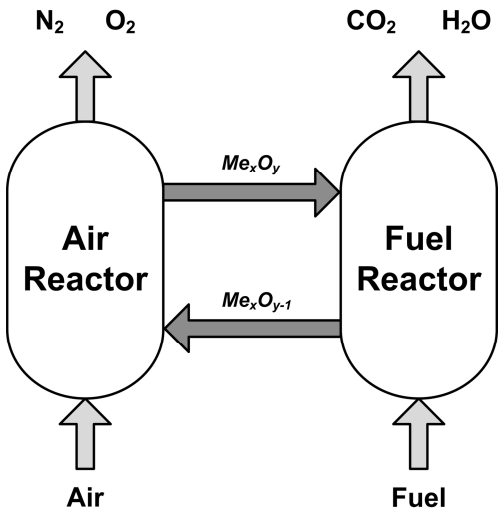


**Figure 1.** Scheme of the Chemical-looping Combustion (CLC) process.

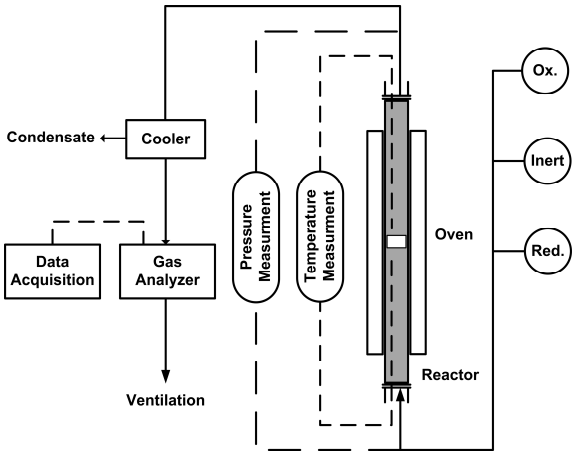


**Figure 2.** Scheme of the experimental setup used in this investigation.

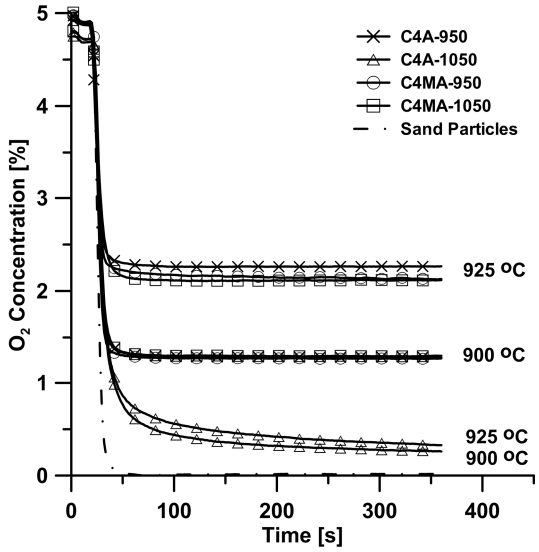


**Figure 3.** Oxygen concentration of C4A and C4MA oxygen carriers during inert gas cycles at 900 and 925°C.

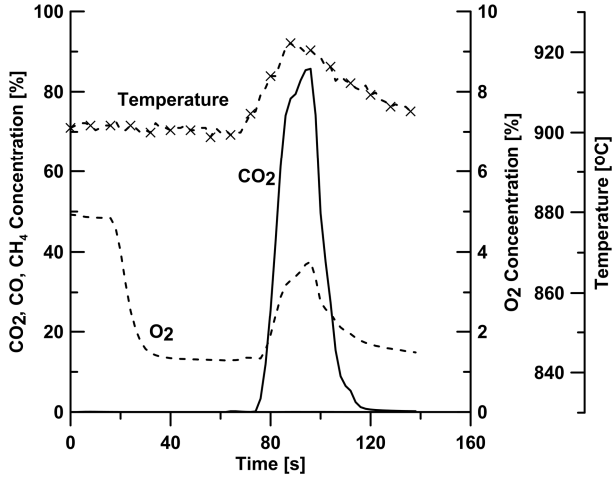


**Figure 4.** Time-dependent concentration and temperature profile for C4A-950 during reduction cycle at 900°C.

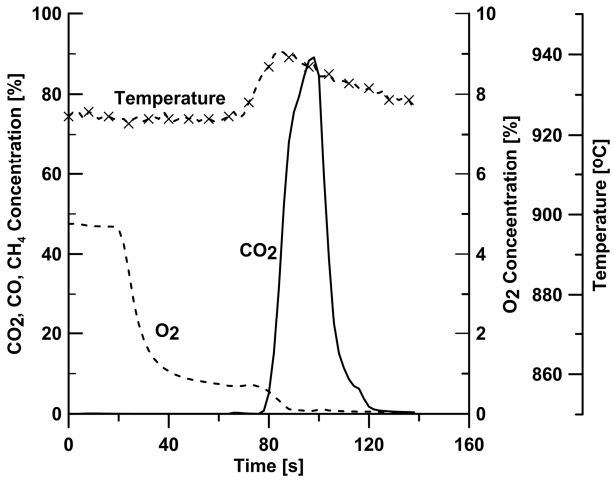


**Figure 5.** Time-dependent concentration and temperature profile for C4A-1050 during reduction cycle at 925°C.

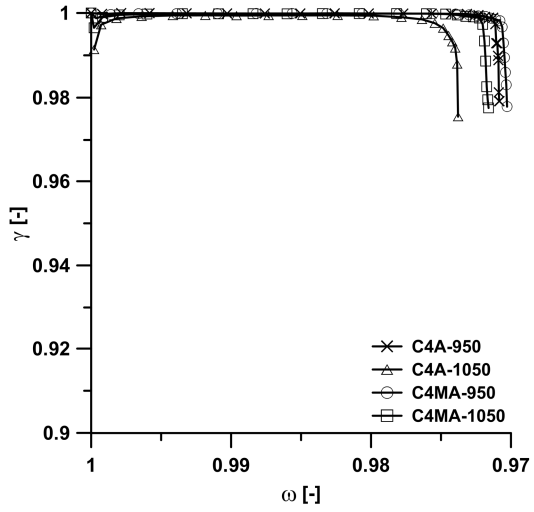


**Figure 6.** Gas yield, γ, as a function of mass-based conversion, $\omega$, for C4A and C4MA oxygen carriers during 20 s of $CH_4$ reduction at 925°C.

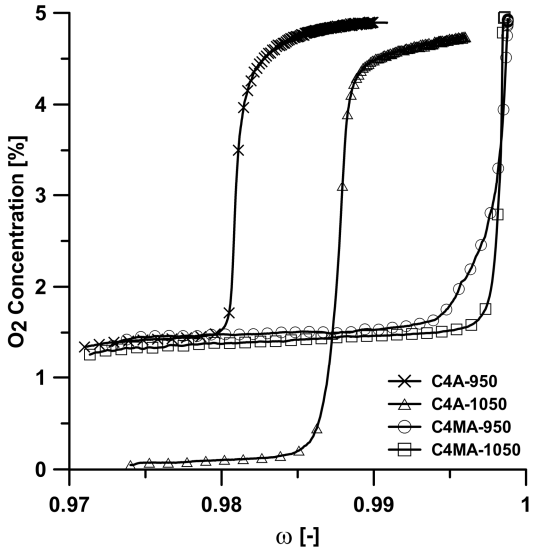


**Figure 7.** Variation of oxygen concentration with mass-based conversion ( $\omega$ ) during oxidation at 900°C for C4A and C4MA oxygen carriers.

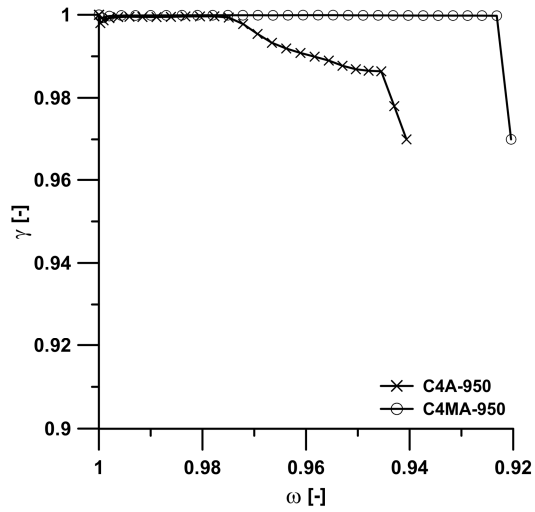


**Figure 8.** Gas yield (γ) as a function of mass-based conversion ( $\omega$ ) for C4A-950 and C4MA-950 oxygen carriers at 925°C during 70 s of $CH_4$ reduction.

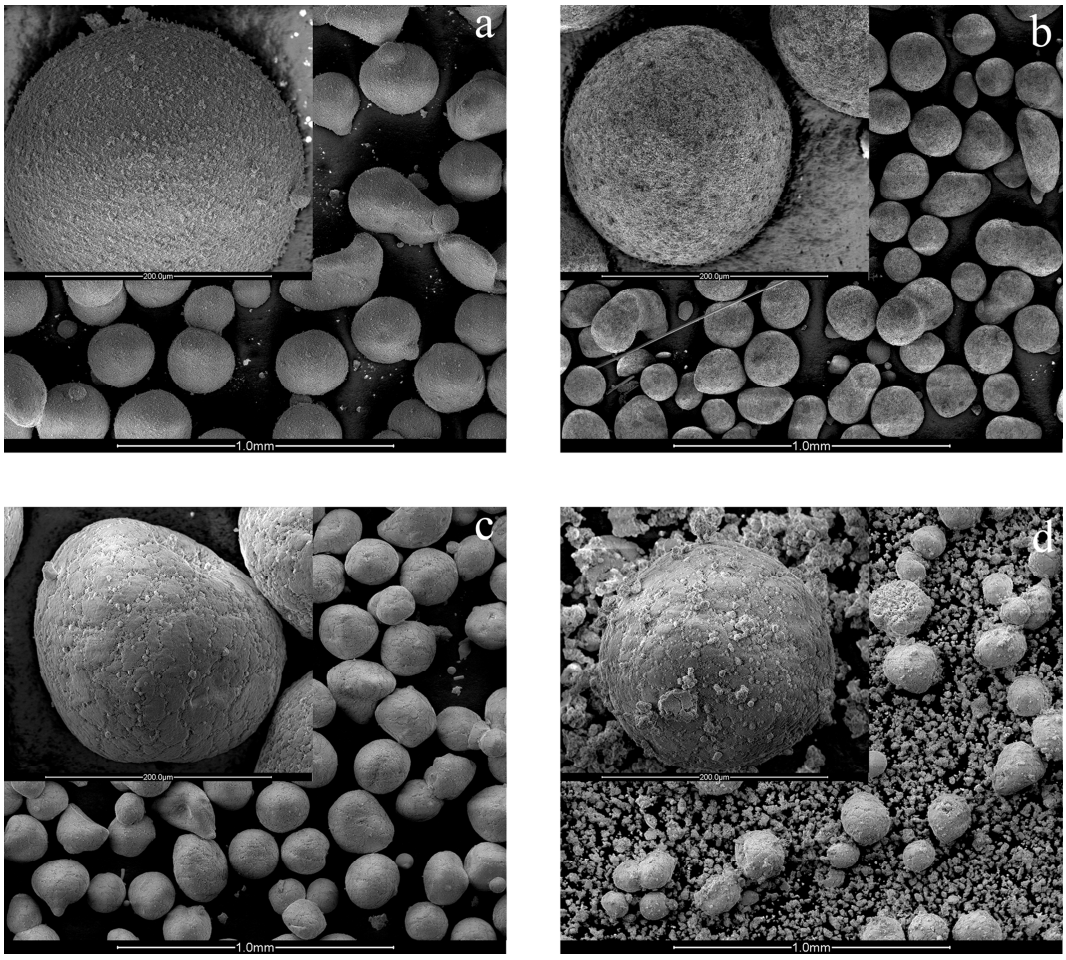


**Figure 9.** ESEM images of (a) C4A-950, (b) C4A-1050, (c) C4MA-950 and (d) C4MA-1050 after reactivity test.

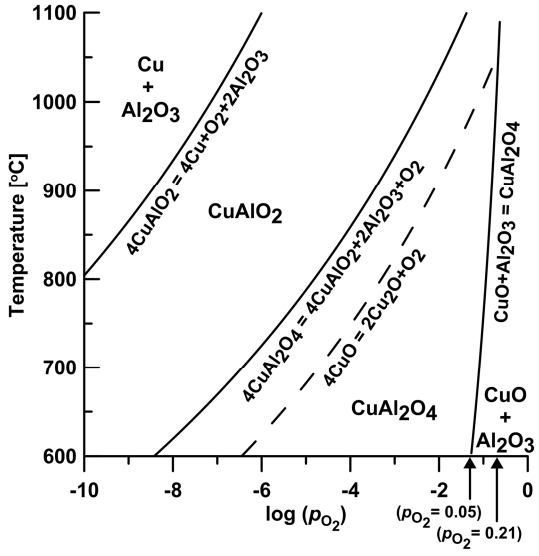


**Figure 10.** Temperature vs. $\log(p_{O_2})$ diagram in the Cu-Al-O system under 1 atm. total pressure.[43]

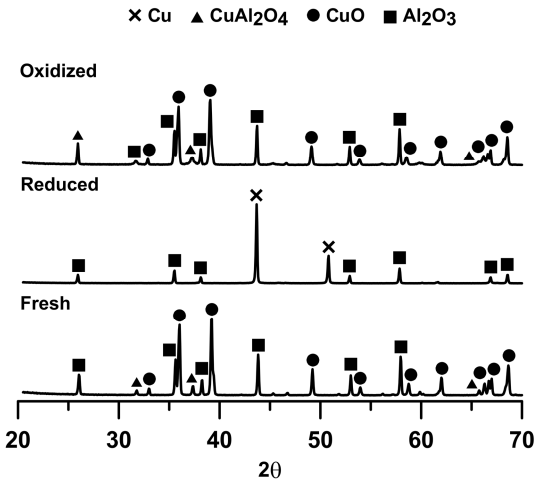


**Figure 11.** Comparative XRD signatures of fresh, $H_2$-reduced and oxidized (5% $O_2$ in $N_2$) samples of C4A-950 at 900°C.

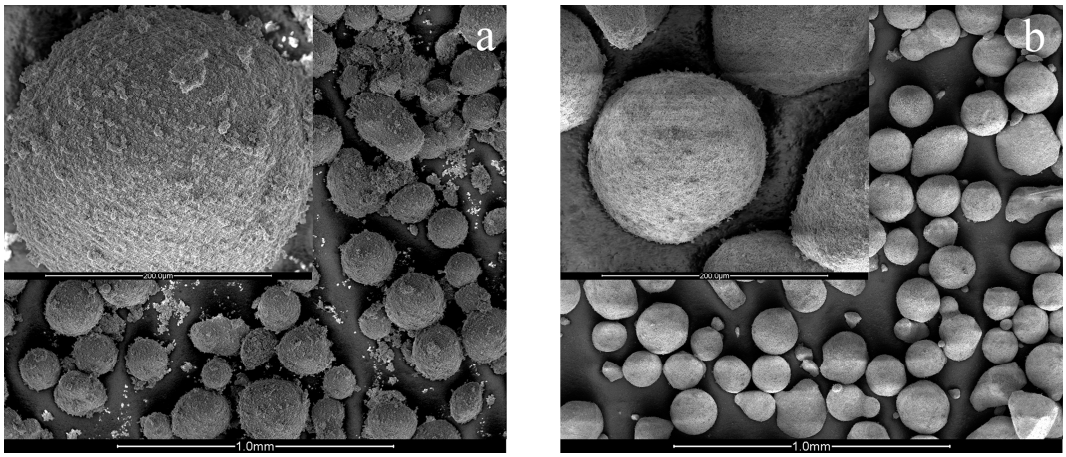


**Figure 12.** ESEM images of oxidized (a) C4A-950 and (b) C4A-1050 subsequent to full reduction using $H_2$. Note the agglomeration in (a) caused by the complete reduction of the oxygen carrier.

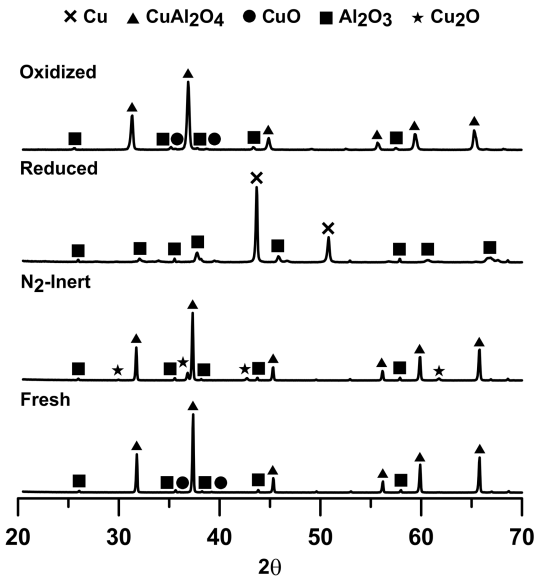


**Figure 13.** Comparative XRD signatures of fresh, $N_2$-inert exposed, $H_2$-reduced and oxidized (5% $O_2$ in $N_2$) samples of C4A-1050 at 900°C.

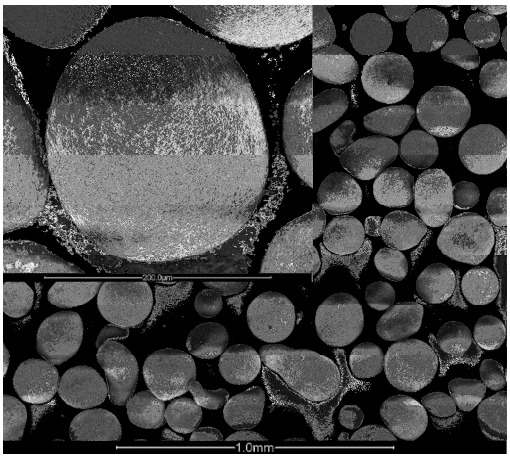


**Figure 14.** ESEM images of C4A-1050 subjected to multi-cycle test of full reduction in methane followed by oxidation.